

MonoForce: Self-supervised learning of physics-aware grey-box model for predicting the robot-terrain interaction

Ruslan Agishev, Karel Zimmermann, Martin Pecka and Tomáš Svoboda

Abstract—We introduce an explainable, physics-aware, and end-to-end differentiable model which predicts the outcome of robot-terrain interaction from camera images. The proposed MonoForce model consists of a black-box module, which predicts robot-terrain interaction forces from the onboard camera, followed by a white-box module, which transforms these forces through the laws of classical mechanics into the predicted trajectories. As the white-box model is implemented as a differentiable ODE solver, it enables measuring the physical consistency between predicted forces and ground-truth trajectories of the robot. Consequently, it creates a self-supervised loss similar to MonoDepth. To facilitate the reproducibility of the paper, we provide the source code. See the project github¹ for codes and supplementary materials such as videos and data sequences.

I. INTRODUCTION

The ability to predict the outcome of robot-terrain interaction from onboard camera images is essential for many fundamental functionalities of autonomous navigation, such as planning or control. Over the last few decades, roboticists proposed a wide variety of *white-box* [1], [2] and *black-box* models [3], [4], each with its strengths and weaknesses. While the white-box models typically suffer from oversimplifications and inability to adapt to a new domain without massive hand tuning, the black-box models suffer from poor generalization, weak explainability, and the need to gather expensive training data when re-trained. We propose to get the best of both worlds by introducing a *grey-box*, explainable, physics-aware, and end-to-end differentiable model that enables self-supervised learning.

We emphasize that generalization is much more crucial in learning the motion model since there is an inherent training/testing distribution mismatch due to the natural absence of robot-endangering samples in real training data. In contrast to existing black-box models [3], [4], we argue that any well-generalizing model should be knowledgeable about the white-box laws of classical mechanics, such as (i) if the robot is falling, then its vertical velocity corresponds to the duration of the free-fall or (ii) any contact with the terrain results in forces acting on the robot body. On the other hand,

This work was supported by Czech Science Foundation under Project 20-29531S and by OP VVV MEYS funded project CZ.02.1.01/0.0/0.0/16.019/0000765 “Research Center for Informatics”. R. Agishev and K. Zimmermann were supported by Grant Agency of the CTU Prague under Project SGS22/111/OHK3/2T/13. (Corresponding author: R. Agishev.)

The authors are with the Department of Cybernetics, Faculty of Electrical Engineering, Czech Technical University in Prague, 166 36 Prague, Czech Republic (e-mail: agishrus@fel.cvut.cz; zimmerk@fel.cvut.cz; peckama2@fel.cvut.cz; svobodat@fel.cvut.cz)

¹<https://github.com/ctu-vras/monoforce>

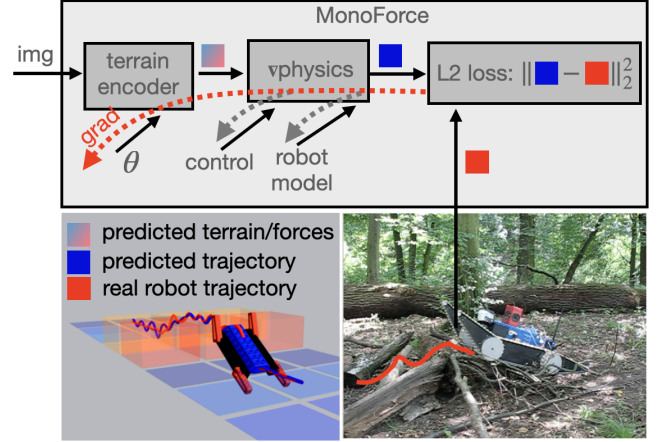


Fig. 1. **MonoForce model:** Terrain encoder is a black-box model that predicts robot-terrain interaction forces. $\nabla\text{physics}$ is the white-box model that computes the robot’s trajectory from forces through the laws of classical mechanics. Self-supervised loss measures physical consistency between forces and ground-truth robot’s trajectory via backpropagation through differentiable physics module.

we still want to employ the black-box model for predicting the size of these forces since they have to be discovered directly from the appearance of contact terrain patches. Consequently, the proposed *MonoForce* model consists of the black-box part (terrain encoder) that predicts the robot-terrain interaction forces, followed by the white-box part ($\nabla\text{physics}$, or *differentiable physics*) that computes the robot motion from the laws of classical mechanics (see Fig. 1 for details). The natural question emerges: “How can we train the terrain encoder?”.

Supervised learning of the terrain encoder is not tractable because the ground truth robot-terrain interaction forces are not directly measurable. At this point, we take inspiration from the well-known MonoDepth model [5] which learns to predict depth in a self-supervised manner by optimizing the *geometrical consistency* between the predicted depth and the image delivered by another calibrated camera onboard. Similarly, we optimize the *physical consistency* between the predicted forces and the robot’s trajectory. This setup is also self-supervised, since locally accurate ground truth robot trajectories can typically be recovered from onboard measurements via a common SLAM procedure.

Towards this end, we train the terrain encoder to predict the latent interaction forces such that when employed in the $\nabla\text{physics}$ module, they generate similar trajectories to the ground truth ones. To proceed with such a physics-supervised

setup, the ∇ physics module is designed as a custom-built differentiable ODE solver similar to NeuralODE [6]. In addition, the resulting model is also directly differentiable with respect to the robot model. Therefore, joint optimization of robot model parameters, such as its center of gravity or moment of inertia, is also possible. The model is also directly differentiable with respect to control; therefore, its plug-and-play usage in state-of-the-art MPC controllers [7] is at hand.

Our main contributions are as follows:

- A novel end-to-end differentiable grey-box model for predicting the robot behavior on complex terrains from camera images.
- A physics-aware, self-supervised learning pipeline that outperforms state-of-the-art kinematics model of Salansky et al. [8].

II. RELATED WORK

Despite being extremely important for predicting robot behaviour on complex terrains, the so far introduced motion models fall unequivocally into one of two categories: white-box or black-box models. We argue that this is one of the most substantial reasons for failure in outdoor robotics. We make the step to fill the grey-zone gap in order to combine the strengths of both types of models.

White-box models [1], [2] often provide good generalizations if prior assumptions, such as the rigidity of the terrain, are satisfied. However, they are usually oversimplified, and the influence of the non-rigid terrain is often ignored completely since it is hard to predict reliably; therefore, their outdoor usage in vegetation-rich environments is typically limited.

Black-box models [3], [4] can be trained on an arbitrary domain; however, the training data are restricted to robot-non-threatening samples. Consequently, either a simulator is leveraged, or the real training set that omits the endangering samples is used. In both cases, a substantial training/testing distribution mismatch is inherently present, which calls for good generalization that is known to be absent in black-box models.

One can bypass this issue by providing manual annotations for real data. For example, Palazzo et al. combined manually annotated real data with a simulator by a domain transfer method [9]. However, manual annotations are extremely expensive. Another source of cheaper manual annotations are expert driver trajectories, that can be used to learn to predict costmap under the inverse reinforcement learning setup [10]. Although the IRL can theoretically learn from robot-endangering samples, since the driver will avoid them, the IRL is often ill-conditioned and the assumption that the driver provides optimal trajectories with respect to a latent cost is often violated. Although the manually supervised approach will always be superior to self-supervised methods (if a sufficient amount of manually annotated data is provided), we do not consider it to be a direct competitor to the proposed method because the manual annotations do not scale well and cannot be easily transferred among different domains (environments and robots).

Finally, the proposed ∇ physics module is implemented as a differentiable ODE solver. The existing end-to-end differentiable physics solvers include Neural ODE framework [6] or differentiable simulators such as Google’s brax [11] or Nvidia’s WARP [12]. While the feedforward pass is usually based on the Runge-Kutta integrator with a dynamic temporal step, backpropagation through physics is typically tackled by the implicit function theorem. We found out that for our task, the custom-built Euler integrator with fixed temporal step delivers similar accuracy while being approximately $10\times$ faster; see comparison with [6] in the experiments section.

III. THEORY

While terrain encoder is a common deep convolutional network based on MonoLayout architecture [13], this section mainly focuses on possible architectures of the ∇ physics module. In general, the higher the complexity of the model, the more complicated physical interactions can be modeled, but the higher the risk of overfitting. Too complex models require detailed inputs such as the complete topological structure and elasticity properties of the vegetation in front of the robot, which cannot be reconstructed from a single camera image. To find a good trade-off between the complexity and the overfitting predispositions, we introduce a set of physics models with increasing complexity.

A. Rigid body motion induced by external forces

We model the robot as a rigid body represented by a set of mass points $\mathcal{P} = \{(\mathbf{p}_i, m_i) \mid \mathbf{p}_i \in \mathbb{R}^3, m_i \in \mathbb{R}^+, i = 1 \dots N\}$, where \mathbf{p}_i denotes coordinates of the i -th 3D point and m_i its mass. The simplest 6DOF motion equations of a rigid body [14] are as follows:

Linear motion:

$$\dot{\mathbf{x}} = \mathbf{v} \quad (1)$$

$$\dot{\mathbf{v}} = \frac{1}{M} \sum_i \mathbf{f}_i \quad (2)$$

Angular motion:

$$\dot{\mathbf{R}} = \boldsymbol{\omega} \times \mathbf{R} \quad (3)$$

$$\dot{\boldsymbol{\omega}} = \mathbf{J}^{-1} \sum_i \mathbf{p}_i \times \mathbf{f}_i \quad (4)$$

where $\mathbf{x}, \mathbf{v} \in \mathbb{R}^3$ are its position and velocity, $\mathbf{R} \in \mathcal{SO}_3$ is its rotation represented by 3×3 orthogonal matrix and $\boldsymbol{\omega} \in \mathbb{R}^3$ is its angular velocity. We denote $\mathbf{f}_i \in \mathbb{R}^3$ all external forces acting on i -th mass point. Although the forces and the trajectory are assumed to be a function of time, we drop the time index for simplicity. Total mass $M = \sum_i m_i \in \mathbb{R}^+$ and moment of inertia $\mathbf{J} \in \mathbb{R}^{3 \times 3}$ are assumed to be known static parameters of the rigid body since they can be identified independently in laboratory conditions. Note that the proposed framework allows backpropagating the gradient with respect to these quantities, too, which makes them jointly learnable with the terrain encoder. The trajectory of the rigid body is the solution of differential equations (1-4),

that can be obtained by any ODE solver for given external forces and initial state (pose and velocities).

When the robot is moving over a terrain, two types of forces are acting on the point cloud \mathcal{P} representing the robot's body: (i) gravitational forces and (ii) robot-terrain interaction forces. The former is defined as $\mathbf{f}_{gi} = [0, 0, -m_i g]^\top$ and acts on the robot at any time, while the latter is the result of complex physical interactions which are not easy to model explicitly, and it acts only on the robot points that are in contact with terrain.

B. Motion induced by terrain forces

One extreme option is to predict the 3D force vectors \mathbf{f}_i directly by the terrain encoder, but we decided to enforce additional prior assumptions to reduce the risk of overfitting. These prior assumptions stem from a common intuition from interactions with flexible objects. In particular, we assume that magnitude of the force that the terrain is exerting on point $\mathbf{p}_i \in \mathcal{P}$ is proportionally increasing with the deformation of the terrain. Consequently, the terrain encoder does not directly predict the force, but it rather predicts the height of the terrain at which the force starts acting on the robot body $h \in \mathbb{R}$, and the scalar value $e \in \mathbb{R}^+$ that generates force $e\Delta h$ proportional to the robot-terrain penetration Δh . We understand the quantity e as an equivalent of elasticity from Hooke's spring model.

Since such force, without any additional damping, would lead to an infinite bumping of the robot on the terrain, we also introduce a robot-terrain damping coefficient $d \in \mathbb{R}^+$, which similarly reduces the force proportionally to the velocity of the point being in contact with the terrain.

Terrain model: In order to apply these forces, we train the terrain encoder to predict a 3-channel heightmap that contains these quantities (height, elasticity, and damping). The height map is in the robot's coordinate frame from the time the input camera image has been captured. During the solution of differential equations (1-4), we apply forces \mathbf{f}_i computed from the terrain that is in contact with point $\mathbf{p}_i = [\mathbf{p}_{xi}, \mathbf{p}_{yi}, \mathbf{p}_{zi}]^\top$. We will always denote the quantities corresponding to point \mathbf{p}_i as h_i, e_i, d_i . We considered two possible terrain models: (i) piece-wise constant model, in which the corresponding quantity is uniquely determined by rounding $(\mathbf{p}_{xi}, \mathbf{p}_{yi})$ on the heightmap grid and (ii) bilinear model, in which the quantities are estimated by bilinear interpolation from neighboring bins. Since the former exhibited significantly lower stability, less realistic behavior, and diminishing gradients during backpropagation, we stayed with the latter; see Figure 3 for an example of the bilinear terrain model.

Vertical terrain force model: The most naive application of the previously outlined principles assumes that the terrain induces only vertical forces. The vertical force \mathbf{f}_{zi} acting on the i -th point \mathbf{p}_i of the robot body is then computed as follows:

$$\mathbf{f}_{zi} = -m_i g + \begin{cases} e_i(h_i - \mathbf{p}_{zi}) - d_i \dot{\mathbf{p}}_{zi} & \text{if } \mathbf{p}_{zi} \leq h_i \\ 0 & \text{if } \mathbf{p}_{zi} > h_i \end{cases}$$

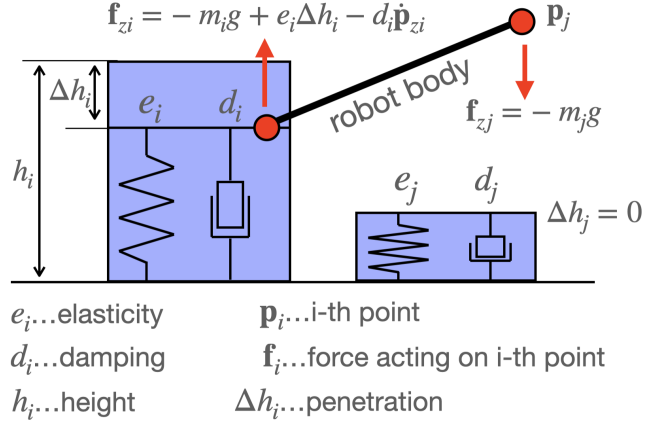


Fig. 2. **Vertical terrain force model:** Simplified 2D sketch demonstrating vertical forces acting on a robot body consisting of two points \mathbf{p}_i and \mathbf{p}_j .

See Figure 2 for a visual sketch of terrain properties and forces on a simplified 2-point robot body. These vertical forces can influence only the robot's roll, pitch, and height; therefore, its initial velocity in $(x, y, \text{heading})$ -space remains constant in the ODE solution.

Normal terrain force model: The more advanced model applies similar forces in the normal direction \mathbf{n}_i of the terrain surface, where the i -th point is in contact with the terrain.

$$\mathbf{f}_i = [0, 0, -m_i g] + \begin{cases} (e_i \Delta h_i - d_i (\dot{\mathbf{p}}_i^\top \mathbf{n}_i)) \mathbf{n}_i & \text{if } \mathbf{p}_{zi} \leq h_i \\ 0 & \text{if } \mathbf{p}_{zi} > h_i \end{cases},$$

where terrain penetration $\Delta h_i = (h_i - \mathbf{p}_{zi}) \mathbf{n}_{zi}$ is estimated by projecting the vertical distance on the normal direction.

C. Motion induced by tracks forces

Our tracked robots move by moving the main tracks and flippers (auxiliary tracks). Flipper motion is purely kinematic in our model. It means that in a given time instant, their pose is uniquely determined by a 4-dimensional vector of their rotations, and they are treated as a rigid part of the robot.

There are several ways to control the robot's motion. During waypoint navigation (which has been used during our data gathering), the speed of the main tracks is controlled by a proportional controller that controls the heading and pose of the robot in order to minimize the difference from a desired waypoint. We consider this controller to be part of the motion model and implement the proportional controller as a part of the model. In such a setup, we assume that the robot's motion is controlled by a user-provided waypoint $\mathbf{u} = [x^g, y^g, \phi^g]$, where ϕ^g stands for desired heading. The robot's angular and linear velocity induced by controlling its tracks by the P-controller are as follows:

$$\mathbf{v}_t(\mathbf{x}, \mathbf{u}) = v \begin{bmatrix} \cos \phi \\ \sin \phi \\ 0 \end{bmatrix}, \quad (5)$$

where $v = \min(K_v \left\| \begin{bmatrix} x - x^g \\ y - y^g \end{bmatrix} \right\|, v_{max})$ and

$$\omega_t(\mathbf{x}, \mathbf{u}) = [0, 0, \min(K_\theta \Delta\theta + K_\phi \Delta\phi, \omega_{max})]^\top, \quad (6)$$

where $\Delta\theta = \arctan(\frac{y^g - y}{x^g - x}) - \phi$ and $\Delta\phi = \phi^g - \phi$ represent accordingly goal point heading difference wrt robot pose and yaw difference. In the equations, K_v , K_θ , and K_ϕ are the controller parameters.

D. Structure of the final model

The resulting ∇ physics module that combines terrain and track forces is the solution of the following ODE:

Linear motion:

$$\dot{\mathbf{x}} = \mathbf{v} + \mathbf{v}_t(\mathbf{x}, \mathbf{u}) \quad (7)$$

$$\dot{\mathbf{v}} = \frac{1}{M} \sum_i \mathbf{f}_i \quad (8)$$

Angular motion:

$$\dot{\mathbf{R}} = (\boldsymbol{\omega} + \boldsymbol{\omega}_t(\mathbf{x}, \mathbf{u})) \times \mathbf{R} \quad (9)$$

$$\dot{\boldsymbol{\omega}} = \mathbf{J}^{-1} \sum_i \mathbf{p}_i \times \mathbf{f}_i \quad (10)$$

The resulting motion model accepts the camera image I representing the state of the environment, current state of the robot $\mathbf{s}_0 = [\mathbf{x}_0, \mathbf{v}_0, \mathbf{R}_0, \boldsymbol{\omega}_0]$, and waypoint \mathbf{u} representing the control signal. Then the terrain encoder predicts the terrain properties and the ODE solver provides the expected 12DOF trajectory $\tau = \mathbf{s}_1 \dots \mathbf{s}_T$ (containing poses and velocities in defined time instances) that corresponds to the solution of differential equations (7-10) with appropriate inputs. The motion model can be understood as a function

$$\tau = f_{\mathbf{w}}(\mathbf{s}_0, I, \mathbf{u}), \quad (11)$$

where \mathbf{w} denotes the parameters of terrain encoder. Once trained, this function can be directly usable as a node expansion model in any state-of-the-art planner or terrain traversability predictor (e.g. by thresholding the maximum roll and pitch of the robot in the resulting trajectory). In future work, we will replace the waypoint control with low-level control of track speed, which will, in turn, enable the use of the model in an MDP controller.

E. Terrain Optimization

Since both the terrain encoder and ∇ physics modules are end-to-end differentiable, the learning is formulated as a regression problem that minimizes the L2-distance between the predicted τ and ground truth τ^{gt} trajectories. The resulting loss

$$\mathcal{L}(\mathbf{w}) = \sum_i \|f_{\mathbf{w}}(\mathbf{s}_i, I_i, \mathbf{u}_i) - \tau_i^{\text{gt}}\|^2$$

measures the physical consistency between robot-terrain interaction forces predicted by the terrain encoder and ground truth trajectories observed on the real robot. The overall learning behavior (speed and convergence) is mainly determined by (i) the way the differentiable ODE solver is implemented and (ii) the horizon over which the difference

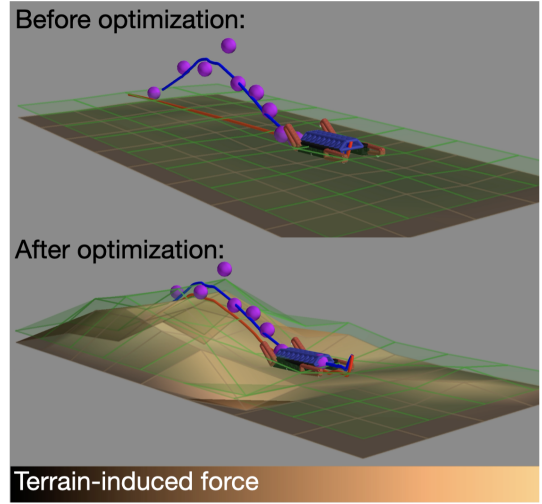


Fig. 3. **Terrain optimized from scratch:** Shape of the terrain (border of the area where terrain forces start to act) outlined by mesh and interaction forces outlined by different colors. The predicted trajectory is in red, and the ground truth trajectory is in blue.

between trajectories is optimized (i.e., the distance of control waypoints from the initial state).

Differentiable implementation of ODE solver: We implemented the forward model $\dot{\mathbf{s}} = g(\mathbf{s}, \mathbf{u})$ corresponding to differential equations (7-10) in PyTorch. We experimented with two possible implementations of the ODE solver. The first one was based on the Neural ODE framework [6]. This implementation leverages the existing ODE solver available in Scipy. The backward pass is computed by calling the solver on the adjoint ODE constructed through PyTorch's autodiff functionality. The second implementation directly implements the Euler integration method with a fixed step size in PyTorch that builds the full computational graph of the integration and then uses the autodiff functionality to get the gradient. Since the former turned out to be significantly faster and achieved comparable accuracy, we employed it for most of our experiments.

Prediction horizon: The length of the horizon employed in learning should correspond to the horizon at which the method is intended to be used. Nevertheless, we observed that both of the previous implementations suffered from diminishing gradients when the horizon was too long. Consequently, we split the training trajectories into 1-second-long chunks and optimized the loss on these data.

F. Terrain Encoder

The optimized terrain shape is used as a label to train the terrain shape predictor. This model takes as input an RGB image and predicts the shape of the supporting terrain in front of the robot. The model can be described as the following function:

$$\hat{\mathcal{H}} = h_{\mathbf{w}}(I) \quad (12)$$

The height map estimate by the model is denoted by $\hat{\mathcal{H}}$, while \mathbf{w} is a vector of the model weights, and I stands for the

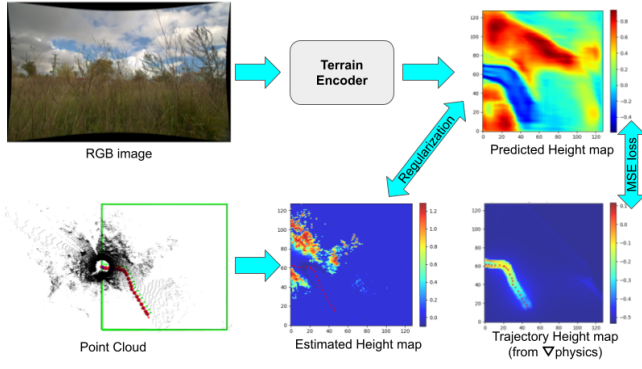


Fig. 4. Terrain encoder training scheme. The *Terrain Encoder* CNN takes as input an RGB image and provides an estimate of the terrain shape in front of the robot. We compare the predicted height map to the optimized height map for the corresponding robot trajectory (according to the method described in Section III-E). Additionally, the regularization signal is computed as a difference between the predicted terrain and the one estimated from the corresponding lidar point cloud. The robot’s trajectory is drawn in red in the top left of the figure alongside the lidar scan. The green box denotes the height map prediction region in front of the robot.

input RGB image. Lidar scans are used in order to provide height map estimates serving as a regularization factor during training, see Figure 4.

As it was studied ([15], [8], [4]), oftentimes a measured by onboard sensors (such as lidar) terrain does not align with the true supporting surface (example on Figure 6). To this extent, we rely on the robot’s experience by recording traversed trajectories, τ , and obtaining corresponding optimized terrains, $\mathcal{H}(\tau)$. However, only the positive traversability labels are not sufficient for reliable navigation [16]. That is why, to reconstruct a realistic terrain, we additionally add a regularization factor. It is provided as an estimated terrain via lidar point cloud interpolation, $\hat{\mathcal{H}}(\mathcal{P})$, similar to [17]. To put it formally, we optimize the following criterion function:

$$\mathcal{L}(\mathbf{w}) = \|W_\tau(h_{\mathbf{w}}(I) - \mathcal{H}(\tau))\|^2 + \lambda \|h_{\mathbf{w}}(I) - \hat{\mathcal{H}}(\mathcal{P})\|^2 \quad (13)$$

The first term describes the weighted difference between the predicted height map from the RGB image, $h_{\mathbf{w}}(I)$, and the supporting height map for the corresponding trajectory, $\mathcal{H}(\tau)$. W_τ denotes the matrix masking out traversed height map cells by the trajectory τ . The second term is a regularization factor, the influence of which on optimization is moderated by the hyperparameter λ .

The MonoForce equation (11) can be interpreted in the following way:

$$f(\mathbf{s}, I, \mathbf{u}) = \tilde{f}(\mathbf{s}, h_{\mathbf{w}}(I), \mathbf{u}), \quad (14)$$

meaning that the terrain encoder $h_{\mathbf{w}}(I)$ is utilized to provide height map input to $\nabla\text{physics}$ module together with the control inputs \mathbf{u} . Next, the trajectory τ is generated from the state \mathbf{s} for a given time window. The resultant height maps are used further as an input to the $\nabla\text{physics}$ module.

IV. EXPERIMENTS

A. Data Collection

We run the experiment on a real data set containing sensory data from forest and field scenarios recorded with the two robot platforms *tracked* (MARV robot, see Figure 6), *wheeled* (Clearpath Husky robot). The data set contains point cloud scans, corresponding images from 4 cameras installed on the robots (front, rear, left, and right), robot trajectories with a 10 s length. We record point clouds, and robot trajectories with the help of SLAM [18] method. Our point cloud data were captured with mobile robots equipped with high-resolution Ouster OS0-128 LiDAR in forest and field environments.

We consider as a main contribution of the released data sequences the introduction of terrain shapes available for the corresponding trajectories. An example of a supporting height map for a traversed path is given in the bottom right corner of Figure 4. The stored terrain is defined as a height map layer (2.5-dimensional surface). With the help of the $\nabla\text{physics}$ module, we obtain height values for each cell of the terrain traversed by a robot following a 10s-long trajectory. The height values are being optimized in such a way that the predicted (by the $\nabla\text{physics}$ module) trajectory is as close as possible to the ground-truth one, as described in Section III-E.

In our experiments, we utilize the Monolayout [13] model as the terrain encoder (12). During the training of the model, we utilized the two data sequences recorded in a forest environment and one in the field. In total, they contain 592 point clouds and corresponding trajectories and images. The data is split into training (with 518 data samples) and validation (with 74 data samples) sets. The best-performing model on the validation set is selected for the evaluation. Qualitative examples of the model performance are given in Figure 5. The predicted height map is compared to the one estimated from the point cloud. It could be noticed that the height map is smoother and provides terrain shape predictions for the regions that were not mapped with the lidar scan. It is beneficial for robust trajectory planning.

B. Trajectory Tracking Accuracy

Experiments are conducted according to the pipeline represented in Figure 1. As the terrain encoder, the three methods are compared, namely:

- height map interpolation from a lidar scan (point cloud) [17],
- terrain prediction model introduced in [8],
- terrain encoder (12) trained according to the scheme described in Section III-F.

Given the supporting terrain shape, robot model, and a sequence of control commands driving the robot, the $\nabla\text{physics}$ module outputs the predicted trajectory, τ . This trajectory is then compared to a real one from the data set (recorded with the SLAM pipeline [18]), τ^{gt} . Table I contains the results for different terrain encoders. We compute mean translation and

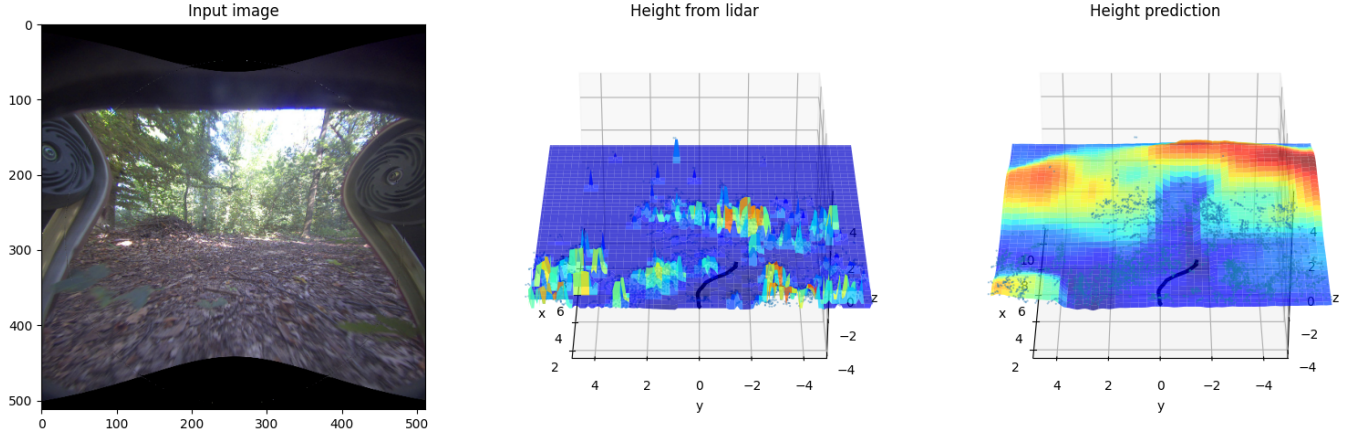


Fig. 5. Terrain encoder (12) prediction example. *Left*: input undistorted RGB image from a front robot camera. *Middle*: height map estimated from a lidar point cloud. *Right*: height map predicted by the model.

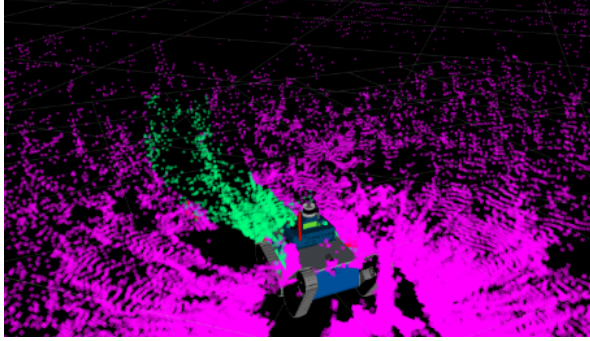


Fig. 6. Tracked robotic platform in a field environment. The green part of the point cloud scan corresponds to the traversed trajectory.

orientation errors for robot locations for the time moments corresponding to the ground truth poses, $t \in (1 \dots T)$.

$$\Delta \mathbf{x} = \frac{1}{N} \sum_{t=1}^T \|\mathbf{x}_t - \mathbf{x}_t^{gt}\| \quad (15)$$

$$\Delta \mathbf{R} = \frac{1}{N} \sum_{t=1}^T \arccos \frac{\text{tr}(\mathbf{R}_t^T \mathbf{R}_t^{gt}) - 1}{2} \quad (16)$$

It can be noticed that both learning approaches ([8] and $h_w(I)$ (12)) outperform the geometrical method for terrain shape estimation in terms of trajectory tracking accuracy. Better orientation estimation results over the approach [8] could be explained by the fact that during the experiments, only the point cloud input was utilized for model [8]. That means that the soft terrain adjustment part of the network (relying on RGB input) was not involved. It is responsible for the supporting terrain estimation for the height map cells containing vegetation.

V. CONCLUSION

A differentiable robot-terrain interaction system (MonoForce) is introduced that is able to provide physical properties of local terrain and predict feasible robot trajectories

TABLE I
TRAJECTORY TRACKING ACCURACY

sensory input	terrain encoder	$\Delta \mathbf{x}$ [m]	$\Delta \mathbf{R}$ [deg]
point cloud	height map interpolation [17]	0.34	13.53
point cloud	height map prediction [8]	0.24	14.51
RGB image	$h_w(I)$ (12), ours	0.24	11.97

given control commands. The system consists of a CNN terrain encoder and explainable ∇ physics module. The terrain encoder provides terrain shape from a single input RGB image. The differentiable physics part provides feasible predictions of robot's trajectories on the terrain for given control sequences. We demonstrate that the ∇ physics module could be used with various terrain encoders and robot models in a differentiable way (terrain optimization examples). We believe that the explainability of the differentiable physics module is key to training terrain encoders that generalize well. It is demonstrated that the trained terrain encoder provides accurate height maps that in turn allow prediction of correct trajectories.

REFERENCES

- [1] S. Fabian, S. Kohlbrecher, and O. Von Stryk, "Pose prediction for mobile ground robots in uneven terrain based on difference of heightmaps," in *2020 IEEE Int. Symp. on Safety, Security, and Rescue Robotics (SSRR)*, 2020, pp. 49–56.
- [2] S. Dogru and L. Marques, "An improved kinematic model for skid-steered wheeled platforms," *Autonomous Robots*, vol. 45, no. 2, pp. 229–243, 2021.
- [3] L. Wellhausen, A. Dosovitskiy, R. Ranftl, K. Walas, C. Cadena, and M. Hutter, "Where should I walk? Predicting terrain properties from images via self-supervised learning," *IEEE Robotics and Automation Letters*, vol. 4, no. 2, 2019.
- [4] M. Guaman Castro, S. Triest, W. Wang, J. M. Gregory, F. Sanchez, J. G. Rogers III, and S. Scherer, "How does it feel? self-supervised costmap learning for off-road vehicle traversability," in *ICRA*, 2023.
- [5] C. Godard, O. Mac Aodha, M. Firman, and G. J. Brostow, "Digging into self-supervised monocular depth prediction," 2019.
- [6] M. N. Ricky T. Q. Chen, Brandon Amos, "Learning neural event functions for ordinary differential equations," in *ICLR*, 2021.
- [7] B. Amos, I. Jimenez, J. Sacks, B. Boots, and J. Z. Kolter, "Differentiable mpc for end-to-end planning and control," in *Advances in Neural Information Processing Systems*, vol. 31, 2018.

- [8] V. Šalanský, K. Zimmermann, T. Petříček, and T. Svoboda, "Pose consistency KKT-loss for weakly supervised learning of robot-terrain interaction model," *IEEE Robotics and Automation Letters*, vol. 6, no. 3, pp. 5477–5484, 2021.
- [9] S. Palazzo, D. C. Guastella, L. Cantelli, P. Spadaro, F. Rundo, G. Muscato, D. Giordano, and C. Spampinato, "Domain adaptation for outdoor robot traversability estimation from rgb data with safety-preserving loss," *2020 IEEE/RSJ International Conference on Intelligent Robots and Systems (IROS)*, pp. 10014–10021, 2020.
- [10] D. Silver, J. A. Bagnell, and A. Stentz, "Learning from demonstration for autonomous navigation in complex unstructured terrain," *The Int. J. of Robotics Research*, vol. 29, no. 12, pp. 1565–1592, 2010.
- [11] C. D. Freeman, E. Frey, A. Raichuk, S. Girgin, I. Mordatch, and O. Bachem, "Brax - a differentiable physics engine for large scale rigid body simulation," 2021. [Online]. Available: <http://github.com/google/brax>
- [12] M. Macklin, "Warp: A high-performance python framework for gpu simulation and graphics," <https://github.com/nvidia/warp>, March 2022, nVIDIA GPU Technology Conference (GTC).
- [13] K. Mani, S. Daga, S. Garg, S. S. Narasimhan, M. Krishna, and K. M. Jatavallabhula, "Monolayout: Amodal scene layout from a single image," in *The IEEE Winter Conference on Applications of Computer Vision*, 2020, pp. 1689–1697.
- [14] K. Bagi, "The contact dynamics method," in *Computational Modeling of Masonry Structures Using the Discrete Element Method*. IGI Global, 2016, pp. 103–122.
- [15] A. Li, C. Yang, J. Frey, J. Lee, C. Cadena, and M. Hutter, "Seeing through the grass: Semantic pointcloud filter for support surface learning," *arXiv preprint arXiv:2305.07995*, 2023.
- [16] J. Bae, J. Seo, T. Kim, H.-g. Jeon, K. Kwak, and I. Shim, "Uncertainty reduction for 3d point cloud self-supervised traversability estimation," *arXiv preprint arXiv:2211.11201*, 2022.
- [17] Y. Wang, H. Li, X. Ning, and Z. Shi, "A new interpolation method in mesh reconstruction from 3d point cloud," in *Proceedings of the 10th International Conference on Virtual Reality Continuum and Its Applications in Industry*, 2011, pp. 235–242.
- [18] F. Pomerleau, F. Colas, R. Siegwart, and S. Magnenat, "Comparing ICP variants on real-world data sets," *Autonomous Robots*, vol. 34, no. 3, pp. 133–148, 2013. [Online]. Available: <https://doi.org/10.1007/s10514-013-9327-2>